XVIII.
INQUA BERN 2011
SWITZERLAND

Poster Award
for
Thursday

The winners are:

Encarni Montoya
Romée Kars

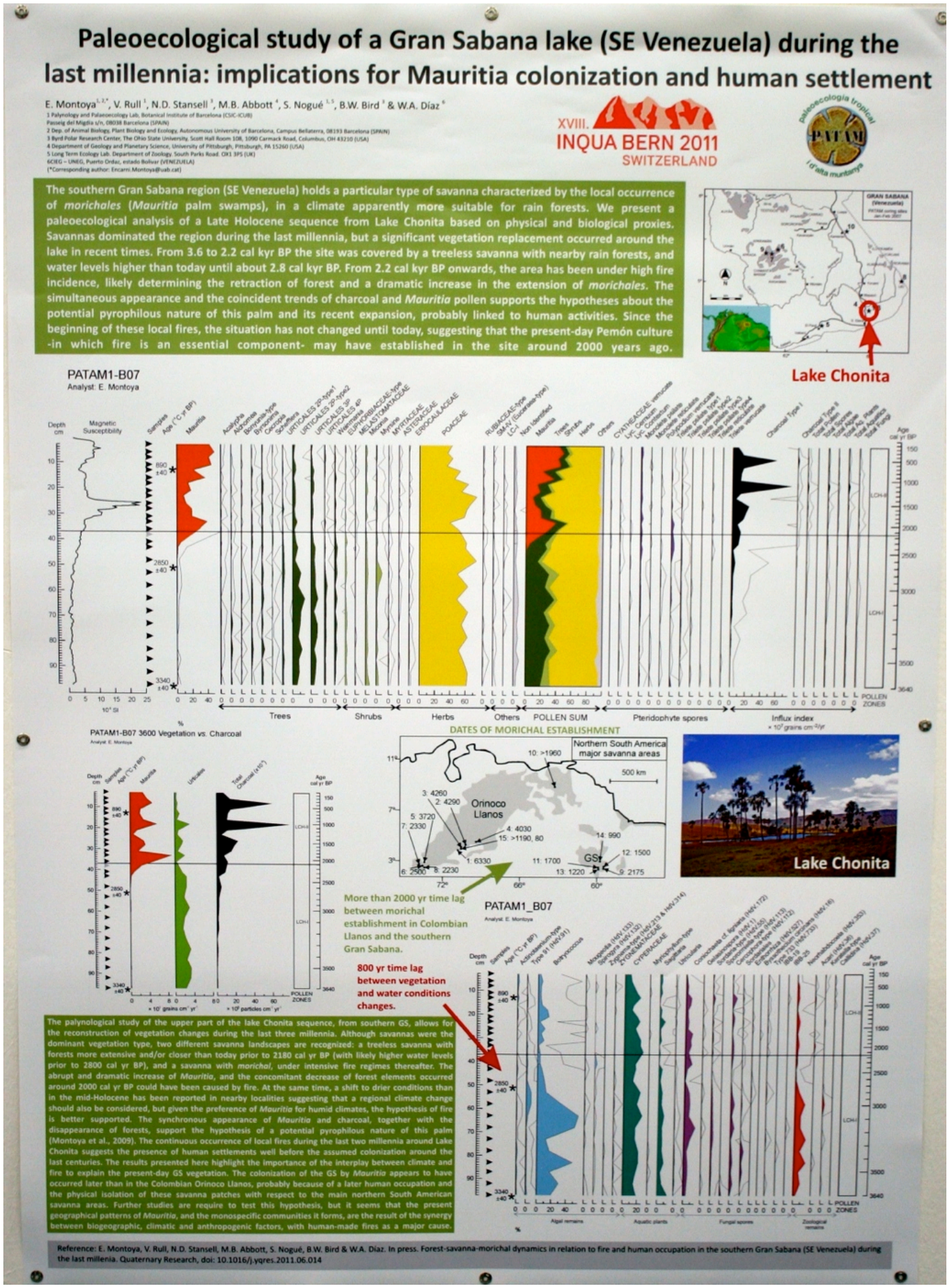

XVIII. INQUA BERN 2011 SWITZERLAND

Poster Award
for
Thursday

Encarni Montoya
Autonomous University of Barcelona
Spain

Sponsor:

sc | nat

Swiss Academy of Sciences
Akademie der Naturwissenschaften
Accademia di scienze naturali
Académie des sciences naturelles

ProClim

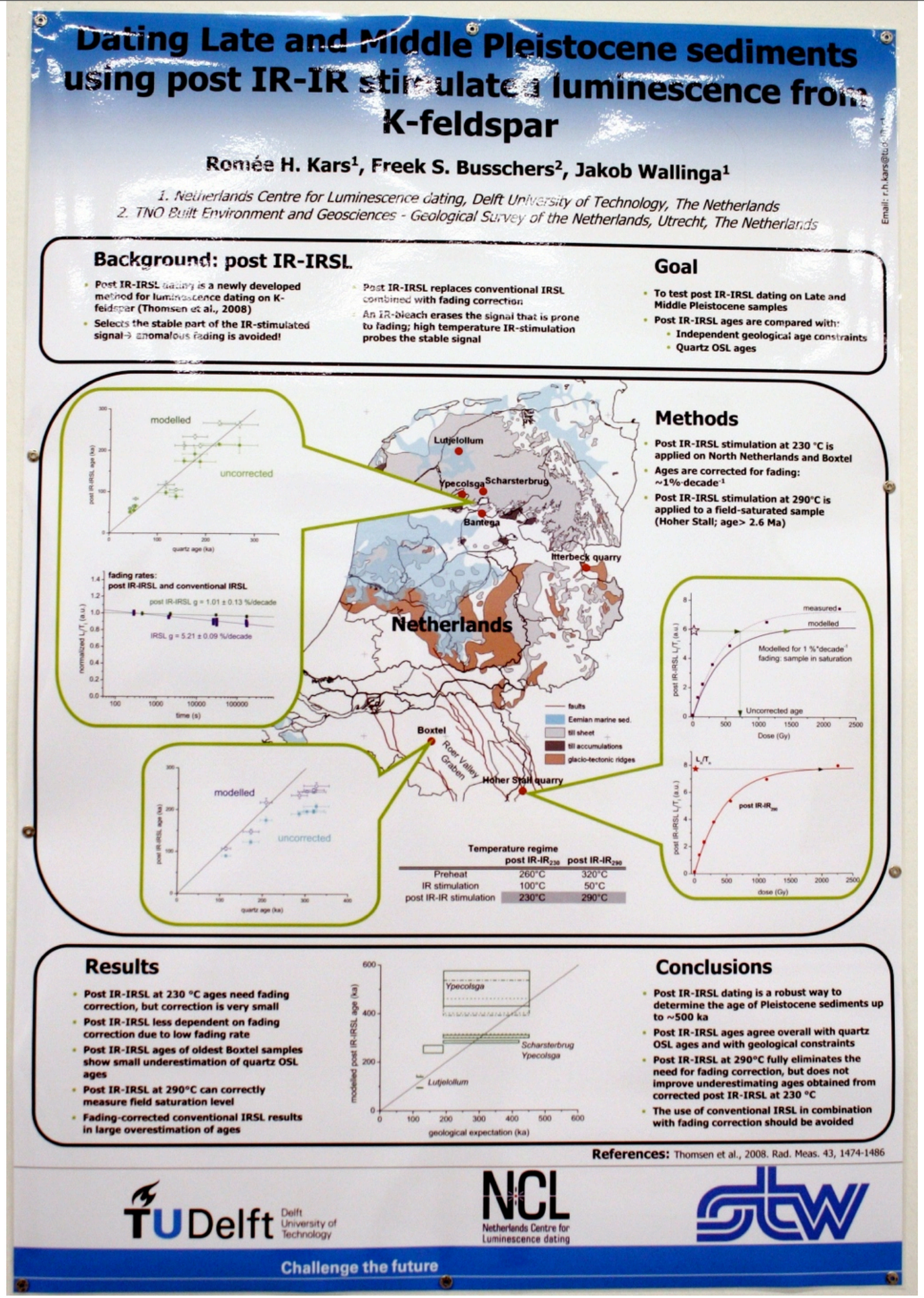

XVIII. INQUA BERN 2011 SWITZERLAND

Poster Award for Thursday

Romée Kars

Delft University of Technology
Netherlands

Sponsor:

sc | nat

Swiss Academy of Sciences
Akademie der Naturwissenschaften
Accademia di scienze naturali
Académie des sciences naturelles

ProClim

XVIII.
INQUA BERN 2011
SWITZERLAND

Poster Award
for
Friday

The winners are:

M.C. Manoj
Lisa Schüler
Elisabeth Dietze

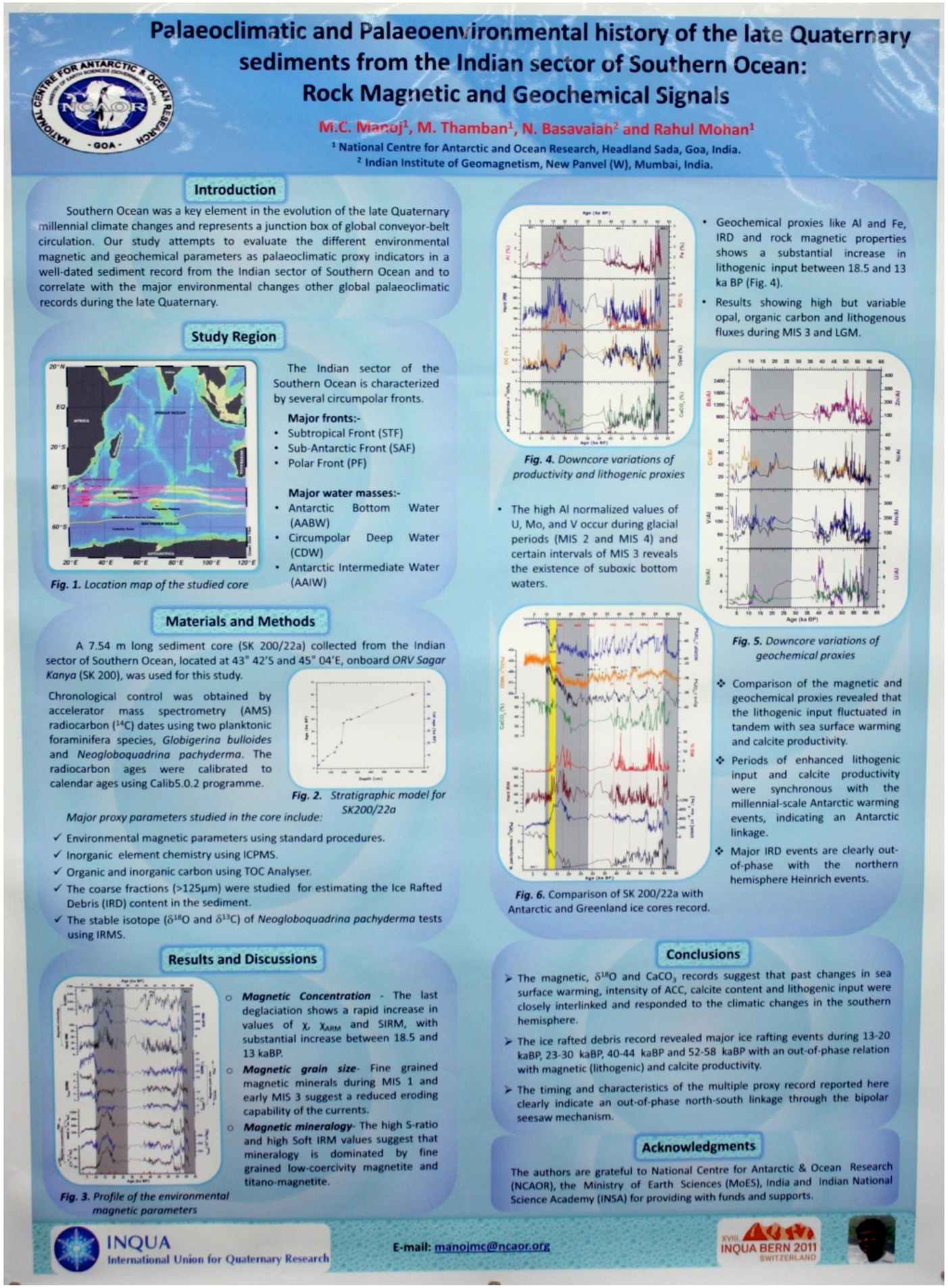

Palaeoclimatic and Palaeoenvironmental history of the late Quaternary sediments from the Indian sector of Southern Ocean: Rock Magnetic and Geochemical Signals

M.C. Manoj[1], M. Thamban[1], N. Basavaiah[2] and Rahul Mohan[1]

[1] National Centre for Antarctic and Ocean Research, Headland Sada, Goa, India.
[2] Indian Institute of Geomagnetism, New Panvel (W), Mumbai, India.

Introduction

Southern Ocean was a key element in the evolution of the late Quaternary millennial climate changes and represents a junction box of global conveyor-belt circulation. Our study attempts to evaluate the different environmental magnetic and geochemical parameters as palaeoclimatic proxy indicators in a well-dated sediment record from the Indian sector of Southern Ocean and to correlate with the major environmental changes other global palaeoclimatic records during the late Quaternary.

Study Region

The Indian sector of the Southern Ocean is characterized by several circumpolar fronts.

Major fronts:-

- Subtropical Front (STF)
- Sub-Antarctic Front (SAF)
- Polar Front (PF)

Major water masses:-

- Antarctic Bottom Water (AABW)
- Circumpolar Deep Water (CDW)
- Antarctic Intermediate Water (AAIW)

Fig. 1. *Location map of the studied core*

Materials and Methods

A 7.54 m long sediment core (SK 200/22a) collected from the Indian sector of Southern Ocean, located at 43° 42'S and 45° 04'E, onboard *ORV Sagar Kanya* (SK 200), was used for this study.

Chronological control was obtained by accelerator mass spectrometry (AMS) radiocarbon (^{14}C) dates using two planktonic foraminifera species, *Globigerina bulloides* and *Neogloboquadrina pachyderma*. The radiocarbon ages were calibrated to calendar ages using Calib5.0.2 programme.

Fig. 2. *Stratigraphic model for SK200/22a*

Major proxy parameters studied in the core include:

- ✓ Environmental magnetic parameters using standard procedures.
- ✓ Inorganic element chemistry using ICPMS.
- ✓ Organic and inorganic carbon using TOC Analyser.
- ✓ The coarse fractions (>125μm) were studied for estimating the Ice Rafted Debris (IRD) content in the sediment.
- ✓ The stable isotope ($\delta^{18}O$ and $\delta^{13}C$) of *Neogloboquadrina pachyderma* tests using IRMS.

Results and Discussions

Fig. 3. *Profile of the environmental magnetic parameters*

- ***Magnetic Concentration*** - The last deglaciation shows a rapid increase in values of χ, χ_{ARM} and SIRM, with substantial increase between 18.5 and 13 kaBP.
- ***Magnetic grain size***- Fine grained magnetic minerals during MIS 1 and early MIS 3 suggest a reduced eroding capability of the currents.
- ***Magnetic mineralogy***- The high S-ratio and high Soft IRM values suggest that mineralogy is dominated by fine grained low-coercivity magnetite and titano-magnetite.

Fig. 4. *Downcore variations of productivity and lithogenic proxies*

- Geochemical proxies like Al and Fe, IRD and rock magnetic properties shows a substantial increase in lithogenic input between 18.5 and 13 ka BP (Fig. 4).
- Results showing high but variable opal, organic carbon and lithogenous fluxes during MIS 3 and LGM.
- The high Al normalized values of U, Mo, and V occur during glacial periods (MIS 2 and MIS 4) and certain intervals of MIS 3 reveals the existence of suboxic bottom waters.

Fig. 5. *Downcore variations of geochemical proxies*

Fig. 6. Comparison of SK 200/22a with Antarctic and Greenland ice cores record.

- ❖ Comparison of the magnetic and geochemical proxies revealed that the lithogenic input fluctuated in tandem with sea surface warming and calcite productivity.
- ❖ Periods of enhanced lithogenic input and calcite productivity were synchronous with the millennial-scale Antarctic warming events, indicating an Antarctic linkage.
- ❖ Major IRD events are clearly out-of-phase with the northern hemisphere Heinrich events.

Conclusions

- ➢ The magnetic, $\delta^{18}O$ and $CaCO_3$ records suggest that past changes in sea surface warming, intensity of ACC, calcite content and lithogenic input were closely interlinked and responded to the climatic changes in the southern hemisphere.
- ➢ The ice rafted debris record revealed major ice rafting events during 13-20 kaBP, 23-30 kaBP, 40-44 kaBP and 52-58 kaBP with an out-of-phase relation with magnetic (lithogenic) and calcite productivity.
- ➢ The timing and characteristics of the multiple proxy record reported here clearly indicate an out-of-phase north-south linkage through the bipolar seesaw mechanism.

Acknowledgments

The authors are grateful to National Centre for Antarctic & Ocean Research (NCAOR), the Ministry of Earth Sciences (MoES), India and Indian National Science Academy (INSA) for providing with funds and supports.

INQUA International Union for Quaternary Research

E-mail: manojmc@ncaor.org

XVIII. INQUA BERN 2011 SWITZERLAND

Poster Award for Friday

M.C. Manoj

National Centre for Antarctic & Ocean Research
India

Sponsor:

PAGES
PAST GLOBAL CHANGES

A new method to investigate past grassland dynamics in South America based on Poaceae pollen grain size

Lisa Schüler and Hermann Behling

INTRODUCTION

Despite the dominance of grassland ecosystems in South America during the Pleistocene and their high biodiversity, these biomes have recieved little attention so far. Not much is known about their past development, biodiversity and dynamic. However, due to the very uniform morphology of Poaceae pollen grains, it has been impossible so far to investigate palaeo-grassland with a palynological approach. In this innovative pilot study we attempt to distinguish between different South American grassland types in space and time based on morphological pollen characteristics of Poaceae.

Based on these circumstances we formulated the following Research Questions:

1) Is it possible to distinguish between grassland types in South America using quantifiable pollen morphological characteristics of Poaceae?

2) Are there spatial trends or patterns and what could they tell us?

STUDY SITES

20 samples from 4 different grassland-types were investigated:

- *Páramo* in S Ecuador (10 samples)
- *Campos* in S Brazil (6 samples)
- *Campos de Altitude* in SE Brazil (2 samples)
- *Pampa* in Argentina (2 samples)

Fig.1: Sites of investigated grassland types

METHOD

5 parameters of at least 60 grains per sample were measured:

1) grain length
2) grain width
3) pore diameter
4) annulus height
5) annulus width

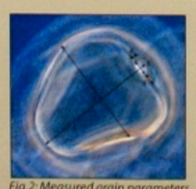

Fig.2: Measured grain parameters

All grains were measured using a photo microscope under 400x magnification. A regression and principle component analysis (PCA) revealed the grain length as a representative parameter and then used for further analyses. The samples per grassland type were pooled. We applied statistical tests and multivariate data analysis to investigate

RESULTS

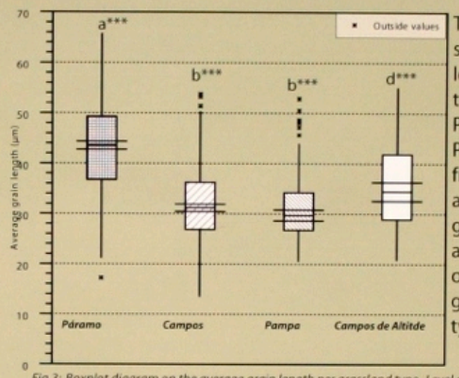

The statistical tests reveal highly significant differences in grain length between all grassland types except for Campos and Pampa (Fig.3). Grains from the Páramo are much larger than from any other grassland. Campos and Pampa have the smallest grains and Campos de Altitude assumes an intermediate position on the size scale. The variation of grain size within one grassland type is rather high.

*Fig.3: Boxplot diagram on the average grain length per grassland type. Level of significance of differences: ***(p<0.001)*

The PCA based on the full dataset with samples shows differences between the grassland types (Fig. 4). The far right position of the Páramo scores is very conspicuous, here the largest pollen grains are found. Also, the highest score density is shifted into the range of larger pollen grains. The smallest grass pollen grains belong to the Campos. Also the other grassland types show distinct grain size distributions.

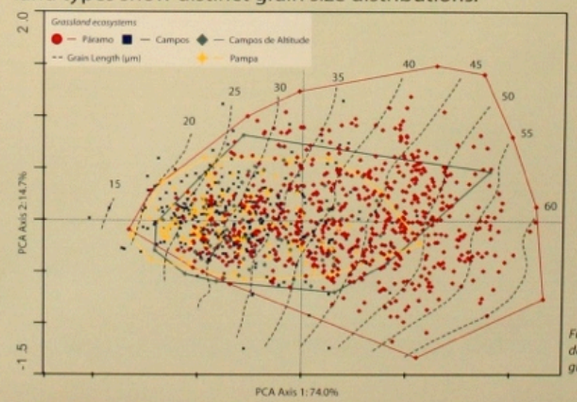

Fig.4: PCA diagram of the full data set with LOESS model of grain length.

CONCLUSION

The results of this pilot study show that it is possible to distinguish between South American grassland types using Poaceae pollen morphology. Assuming that a certain size range corresponds to a certain Poaceae taxa, we can derive different taxa compositions in the different grassland types. From our results we can also assume spatial and temporal patterns e.g. that the Campos taxa composition is more closely related to the one found in Pampa and Campos de Altitude, maybe being even a derivative of these. During cooler periods species from Pampa and Campos de Altitude might have moved to the warmer Campos area, comprising today's taxa composition.

This approach has high potential to unravel so far inaccessable patterns and dynamics of biodiversity and taxa composition of palaeo-grasslands.

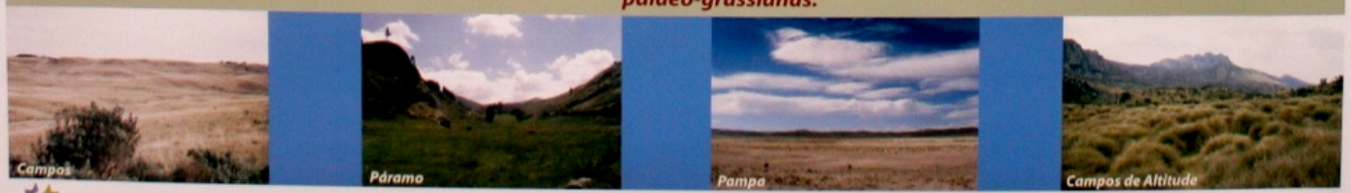

Department of Palynology and Climate Dynamics
Corresponding author: Lisa Schüler
lisa.schueler@biologie.uni-goettingen.de
Göttingen Center for Biodiversity & Ecology
GEORG-AUGUST-UNIVERSITÄT GÖTTINGEN

XVIII. INQUA BERN 2011 SWITZERLAND

Poster Award for Friday

Lisa Schüler

University of Göttingen
Germany

Sponsor:

Stadt Bern

Higher lake stands at Lake Donggi Cona, NE Tibetan Plateau, China

– combining geomorphological and sedimentological approaches

Freie Universität Berlin

E. Dietze[1], B. Wünnemann[1,2], K. Hartmann[1], M. Paprotzki[1], M. Runge[1], G. Lockot[1]

[1] Institute of Geographical Sciences, Interdisciplinary Centre for Ecosystem Dynamics in Central Asia (EDCA);

[2] School of Geography and Oceanography, Nanjing University, China

Background

The project aims to reconstruct the Quaternary landscape evolution of the north-eastern Tibetan Plateau, e.g. within the catchment of Lake Donggi Cona (35.3° N, 98.6° E, 4090 m a.s.l., Fig. 1). Changes in local base level control many geomorphological and sedimentological processes within a lake catchment and, hence, effect proxy generation and conservation in terrestrial archives. Lake level changes below the present level have already been presented in *Dietze et al. (2010)*. *Mischke et al.* (2010) discussed indirect (i.e. ostracod) proxy evidences for lake status changes.
Here, we present a first basin-wide view on higher lake levels from geomorphological and sedimentological evidences.

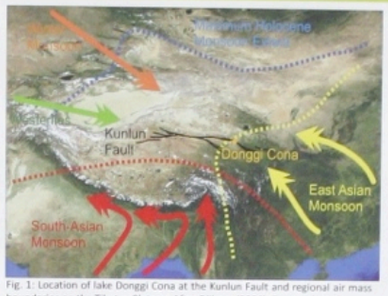

Fig. 1: Location of lake Donggi Cona at the Kunlun Fault and regional air mass boundaries on the Tibetan Plateau. After Böhner (2006), Fu et al. (2005).

Methods

Nine on-shore terrace transects were mapped in detail in their geomorphologic context using tachymetry and differential GPS. On-shore lake sediments were described and sampled at high resolution at several outcrops and pits around the lake (Figs. 3-5).

Volume percentages of 85 grain size classes less than 2 mm were measured with a Coulter LS 200 laser diffraction particle size analyser. Geochemical composition was determined with an ICP-OES device. Future work will include a detailed interpretation of these data sets as they provide important environmental information.

Results

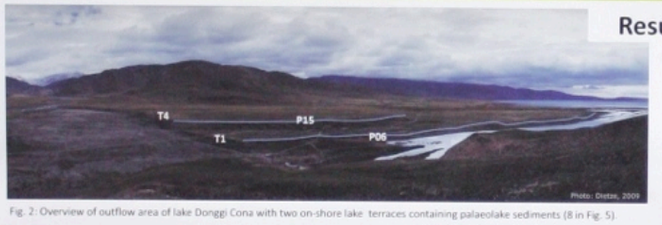

Fig. 2: Overview of outflow area of lake Donggi Cona with two on-shore lake terraces containing palaeolake sediments (8 in Fig. 5).

Fig. 3: Rare example for on-shore terraces (left) on the southern rim of Lake Donggi Cona (6 in Fig. 5), which is dominated by sediment erosion, as shown e.g. by an abrasion platform 10 m above the present lake level (a.p.l.l) (right).

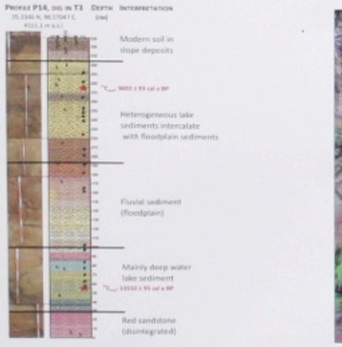

Fig. 4: At profile P14 lake sediments intercalate with floodplain and aeolian sediments at the 2nd largest inflow to lake Donggi Cona.

Fig. 5: Locations of investigated lake sediments (cf. Fig. 6) and terraces above the present level of lake Donggi Cona., NE Tibetan Plateau.

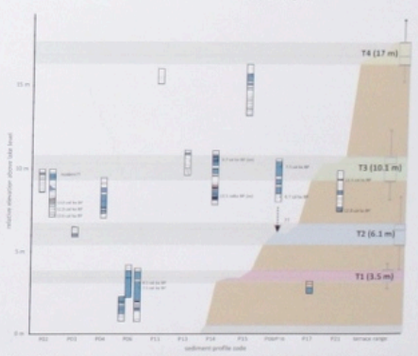

Fig. 6: Sketch of all lake sediment profiles within the range of related terraces above the present lake level. Mean calibrated 14C ages may include a potential reservoir age of ~2000 years.

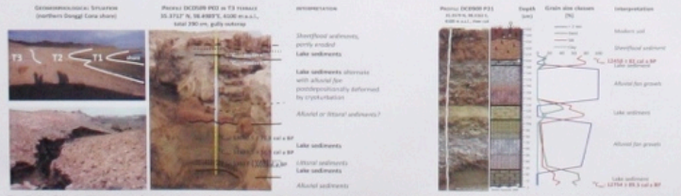

Fig. 7: Profiles in T3 terrace showing intercalation of fluvial/alluvial and lacustrine sediments (P02, P21 in Fig. 5). Grain size distributions in P21 show a high content of silty aeolian material in the lake sediments.

Four on-shore terraces above the present lake level were mapped around the lake, showing different grades of erosion. A vertical displacement by tectonic forcing can be excluded. Lake sediments above the present lake level are intercalated with fluvial, alluvial and littoral sediments at several locations. They give detailed information on environmental processes for the Early and Mid-Holocene time slices. However, they are often discontinuous and post-depositionally overprinted by permafrost and/or earthquakes – allowing only relative reconstructions.

Future work will focus on the interpretation of the lab data. Modelling of grain size end-members with the algorithm of Dietze et al. (in rev., Sed. Geol.) will be combined with the uncertainties in age data, which will lead to new probability-based approaches of interpreting environmental processes.

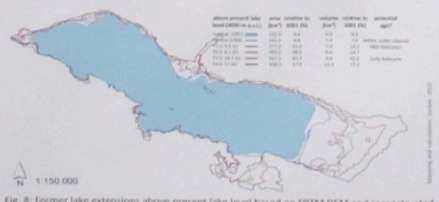

Fig. 8: Former lake extensions above present lake level based on SRTM DEM and reconstructed from geomorphological mapping and remote sensing. Age estimation after Fig. 6.

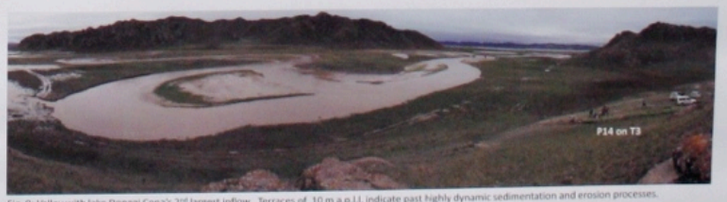

Fig. 9: Valley with lake Donggi Cona's 2nd largest inflow . Terraces of 10 m a.p.l.l, indicate past highly dynamic sedimentation and erosion processes.

Elisabeth Dietze, +49-30-83870254, elisabeth.dietze@fu-berlin.de http://www.cambugan.org

XVIII. INQUA BERN 2011 SWITZERLAND

Poster Award for Friday

Elisabeth Dietze

Free University Berlin
Germany

Sponsor:

nature geoscience

XVIII.
INQUA BERN 2011
SWITZERLAND

Poster Award
for
Saturday

Presented by Steve Colman
PAGES Steering Committee

The winners are:
Esther Haudenschild
Yoshimi Kubota

Cosmogenic ^{10}Be exposure dating of ancient quarries in Western Turkey

Haudenschild Esther, Akçar Naki*, Yavuz Vural**, Ivy-Ochs Susan***, Alfimov Vasily***, Kubik Peter W.***, and Schlüchter Christian**

* Institut für Geologie, Baltzerstrasse 1+3, CH-3012 Bern (e.haudenschild@students.unibe.ch)
** Istanbul Technical University, Faculty of Mines, TR-80626 Maslak, Istanbul
*** Labor für Ionenstrahlphysik (LIP), ETH Zurich, 8093 Zurich, Switzerland

1. Introduction

Kestanbol quartz-monzonite, outcropping in the Ezine village of Çanakkale, Turkey (Fig. 1, Fig. 4) was operated by the Romans for the production and export of building stones since ancient times. Today, remnant building stones can still be found in the ruins of these quarries, whose extent and operation periods are unknown. However, a Roman period can be estimated between 310 BC (Ricl, 1997) to 420 AD (Akçar et al., in prep.), according to the foundation and decay of *Alexandreia Troas*.

Can cosmogenic ^{10}Be help to quantify the chronology of quarrying in this area?

Fig. 1: Location of the study area.

Fig. 2: Sampling sites at Yedi Taşlar quarry with seven columns of 12.5 m length (Akçar et al., in prep.).

Fig. 3: Sampling sites at the quarry near Zurnacıdeğirmeni with columns of 12 m length.

Fig. 4: Overview of study area with sampling sites, mapped area and ancient cities.

2. First ^{10}Be Results

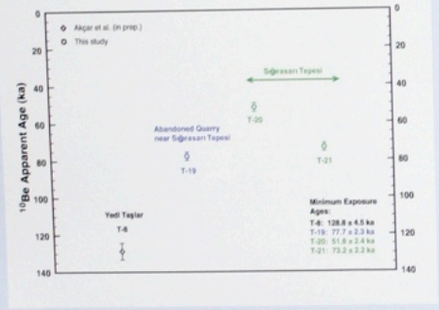

Fig. 5: Comparison of minimum rock surface exposure ages of this study and Akçar et al. (in prep.).

According to our first ^{10}Be results from bedrock samples, the landscape surface in the study area is at least 130 ka old (Fig. 5). The exposure ages of the worked steps at the Yedi Taşlar quarry vary from 7 ka to 10 ka, whereas exposure ages of worked steps at the quarry near Zurnacıdeğirmeni fluctuate between 4 ka and 5 ka (Fig. 6). Despite the difference, both quarries show significantly older ages than 310 BC (Ricl, 1997) to 420 AD (Akçar et al., in prep.) based on archaeological data . Therefore, sampled working steps contain a significant amount of inherited cosmogenic ^{10}Be in our study area.

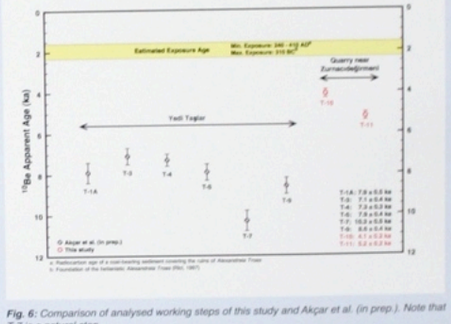

Fig. 6: Comparison of analysed working steps of this study and Akçar et al. (in prep.). Note that T-7 is a natural step.

3. Depth Profiling

As we are not able to directly exposure date operation periods of these quarries, we sampled a recently abandoned quarry at Sığırasarı Tepesi near Akçekeçili to model the variation of ^{10}Be with depth. Eight samples were taken (Fig. 7), analysed and sample depths with corresponding concentrations are plotted in Fig. 8. As we can see is in a depth of 14.5 m still a concentration around 14000 atoms/gram quartz measurable.

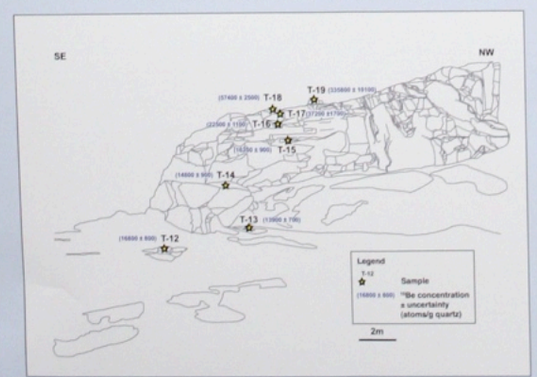

Fig. 7: Depth profiling samples indicated by stars in a recently abandoned quarry at Sığırasarı Tepesi near Akçekeçili. The values in brackets are the measured ^{10}Be concentrations.

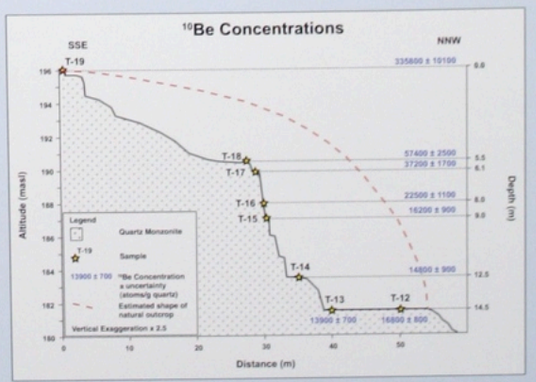

Fig. 8: Depth profiling samples indicated by stars in a recently abandoned quarry at Sığırasarı Tepesi near Akçekeçili. Measured ^{10}Be concentrations are plotted at their corresponding depth. The red dashed line indicates the estimated shape of the natural outcrop.

4. Conclusion

The landscape surface is at least 130 ka old in our study area. Roman quarries in the Kestanbol quartz-monzonite can not directly be exposure dated with in-situ produced cosmogenic ^{10}Be surface exposure dating due to inheritance. Samples for a depth profile show at 14.5 m depth still concentrations of 14000 atoms/gram quartz.

5. Outlook

In the following, a model of the ^{10}Be concentration with depth in the Kestanbol quartz-monzonite will be developped with which we will be able to correct our working step ages for inheritence. Thus, we finally will be able to calculate exposure ages to determine operation periods of Roman quarries in our study area.

6. References

Akçar, N., Yavuz, V., Ivy-Ochs, S., Haudenschild, E., Alfimov, V., Kubic, P.W., in preparation First results on determination of cosmogenic ^{10}Be in antique quarries near Alexandreia Troas (NW Turkey)

Lazzarini, L., 1987. I graniti dei Monumenti Italiani e i loro problemi di deterioramento in: Bureo A., Tabasso, M. L. & Palanzoli G. Materiali Lapi dei it. Bollettino d'Arte Suppl. 41: 157-172

Ricl, M.,1997. The Inscriptions of Alexandreia Troas. Inschriften griechischer Städte aus Kleinasien, Vol. 53. Bonn: Habelt.1 03

7. Acknowledgments

We would like to thank the archaeological museum of Çanakkale and Ismail Hakki Tunçer for their help and cooperation. We would also like to thank Dr. H.-A. Synal and the Laboratory of Ion Beam Physics at ETH Zurich for their support of field work, lab work and AMS measurements. This study was partially funded by SCNAT, Berne University Research Foundation (Project No. 26/09), Istanbul Technical University Research Project (No: 33040) and Swiss National Science Foundation (Project No. 200020-118038 and 200020-111678).

XVIII. INQUA BERN 2011 SWITZERLAND

Poster Award for Saturday

Esther Haudenschild

University of Bern
Switzerland

Sponsor:

Stadt Bern

Millennial-scale variations in East Asian summer monsoon during the last glacial period based on Mg/Ca and oxygen isotope of *Globigerinoides ruber* from the northern East China Sea

ID 2010
Isotope hydrology as a tracer of Quaternar climates

Yoshimi KUBOTA[1], Katsunori KIMOTO[2], Ryuji TADA[1], Masao UCHIDA[3], Ken IKEHARA[4]

1. University of Tokyo, Japan (yoshimi@eps.s.u-tokyo.ac.jp). 2. Japan Agency for Marine-Earth Science and Technology (JAMSTEC) , Japan. 3. National Institute for Environment Studies (NIES), Japan, 4. Geological Survey of Japan, National Institute of Advanced Industrial Science and Technology (AIST), Japan.

Questions

Does sea surface salinity in the northern East China Sea oscillate in harmony with Dansgaard-Oeschgar cycles during Marine Isotope Stage 3?

It has been suggested that changes in fresh water discharge from the Yellow and Yangtze Rivers attributed to deposition of dark and light layers in the Japan Sea, which are in association with Dansgaard-Oeschger (D-O) cycles [Tada et al., 1999]. This study aims to reconstruct sea surface salinity in the northern East China Sea in order to test this scenario.

Oceanography

Fig. 1 Present current system in the East China Sea after Ichikawa and Beardsley [2002] and location of cores KR07-12.

Summer at present

Surface salinity in the northen East China Sea
Discharge of the Yangtze River (Changjiang)
Rainfall in the catchment area of Yangtze River

[Delcroix and Murtugudde, 2002]

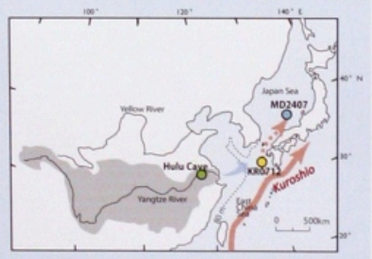

Fig. 2 Locations of the studied site (KR07-12), MD2407 in the Japan Sea [Kido et al.], and Hulu Cave [Wang et al., 2001]. Shaded zone represents the drainage area of the Yangtze River. 80 m sea-level drop corresponds MIS3.

East China Sea to Japan Sea

Temporal variation patterns of oscillations in grayscale (L*) of the hemipelagic sediments in the Japan sea are coincide with the D-O cycles in Greenland ice cores. The grayscale principally reflect organic carbon contents (C_{org}) that was controlled by primary production during the MIS3 [Tada et al., 1999]. Deposition of dark layers contain higher C_{org}, and were attributed to nutreint-rich and low-salinity water from the East China Sea.

Fig. 3 Photo of a sediment in the Japan Sea, water depth of 2074 m.

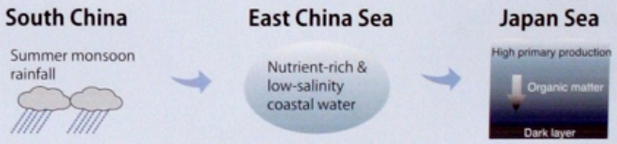

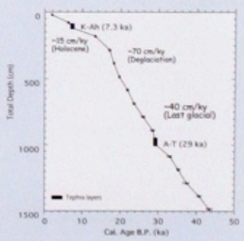

Age model

2~4 mg of planktic foraminifera ***N. dutertrei*** were used for the AMS measurement.

AMS ^{14}C ages were converted to calendar ages by using calib. 6.0 with marine 09 and local reservoir correction of +29 yr.

Fig. 4 A depth versus calendar age for core KR07-12. Error bars show 2σ error. ~15 cm/ky, ~70 cm/ky, ~40 cm/ky are linear sedimentation rate for the Holocene, early deglaciation, the last glacial period, respectively.

Results

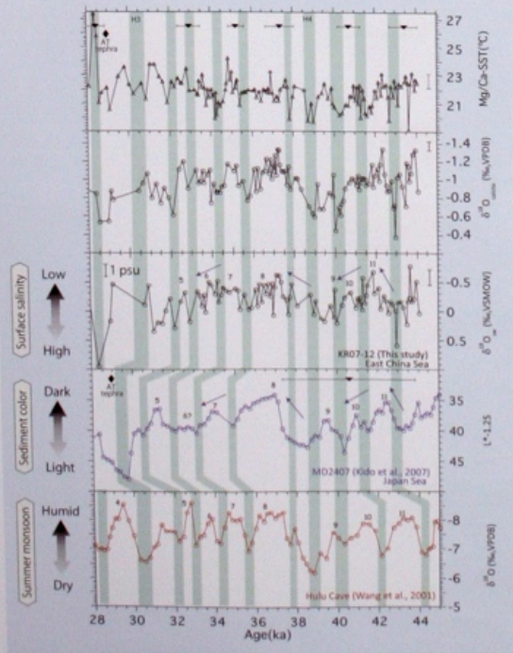

Fig. 7 (a) Mg/Ca-SST of *G. ruber* KR07-12 in the northern East China Sea (this study), (b) $\delta^{18}O$ of calcite *G. ruber* [this study], (c) $\delta^{18}O$ of seawater with global ice volume correction by using a sea-level curve of Waelbroeck et al et al. [2002], (d) L* of MD2407 [Kido et al., 2007], (e) $\delta^{18}O$ of stalagmite record in Hulu Cave [Wang et al., 2001]. Triangles represent ^{14}C age controlling points with 2σ errors. Diamonds show the age controlling points by AT tephra (29 ka). Numbers in figures (c), (d) and (e) represent D-O cycle numbers.

Mg/Ca in fossil foraminiferal calcite

SST = ln (Mg/Ca/ 0.38)/0.089- (1) [Hatings et al., 2001]
SST: Sea surface temperature
※Planktic foraminifera *"G. ruber "*
①Dwelling: upper 30 m in water column
②Season: May to August (Xu et al., 2005)

Oxygen isotope ($\delta^{18}O$)

SST =14.9 - 4.8 ($\delta^{18}O_{calcite}$- $\delta^{18}O_{sw}$)- (2) [Bemis et al., 1998]
$\delta^{18}O_{sw}$: Oxygen isotope of ambient seawater
※Locally, $\delta^{18}O$ is linearly related to sea surface salinity [Oba, 1998].
※Global ice volume effect was corrected by Waelbroeck et al., 2002)

Discussions

①. Approximately 1‰ amplitude of variations in surface salinity variations is equivalent to 5 psu in salinity, if the modern saliniy- $\delta^{18}O_{sw}$ relationship [Oba, 1998] is used.

②. From 44 to 38 ka, millennial-scale variations in $\delta^{18}O_{sw}$ in the northern East China Sea correlate well with those in L* in the Japan Sea, although the interstadial #10 and #11 are ~1 ky younger than those in Hulu Cave due to the error of the age models . Stadial #10 is recognized clearly in the East China Sea and in the Japan Sea, while that is not obvious in Hulu Cave.

1. Temperature

①. SST oscillates by ~3℃ during MIS3
②. Lower SST correspond to Heinrich events #4 and #3, and D-O stadial #5, 6, 7, 10, and 11. It suggests **teleconnection between the East China Sea and north Atlantic climate.**

2. Salinity ($\delta^{18}O_{sw}$)

①. $\delta^{18}O$ of seawater ($\delta^{18}O_{sw}$) oscillates by ~ 1‰ during MIS3.
②. Heavier $\delta^{18}O_{sw}$ corresponds to Heinrich events #4 and stadial #3, 5, 6, 7, 10, and 11.
③. **Temporal variation in $\delta^{18}O_{sw}$ agrees well with that of L* in the Japan Sea,** supporting that the nutrient-rich coastal water of the East China Sea entered to the Japan Sea and caused deposition of dark layers.

③. From 38 to 28 ka, interstadial #6 is obvious in $\delta^{18}O_{sw}$ in the East China Sea while that is not clear in L* of the Japan Sea sediments.

Conclusion

Our results support the idea that the intrusion of the East China Sea coatal water caused repeated deposition of dark layers in the Japan Sea on millennail-scale during MIS 3.

References

Acknowledgment

The travelling and accommodation fees are supported by GCOE of Department of Earth and Planetary Science, University of Tokyo.

XVIII. INQUA BERN 2011 SWITZERLAND

Poster Award for Saturday

Yoshimi Kubota

University of Tokyo
Japan

Sponsor:

PAGES
PAST GLOBAL CHANGES

XVIII.
INQUA BERN 2011
SWITZERLAND

Poster Award
for
Monday

Presented by Christoph Ritz
ProClim- / INQUA LOC

The winners are:
Rebecca Rixon
Nicole Spaulding
Ann Rowan
Nelleke van Asch

Ice-free areas have existed through multiple glacial cycles on the Antarctic Peninsula.

[1]Rebecca Rixon, [2]Christopher Fogwill, [3]Morag Hunter, [4] Pete Convey, [5]Sheng Xu, [5]Finlay Stuart, [5]Christoph Schnabel
[1]University of Exeter, [2]University of New South Wales, [3]Cambridge University, [4]British Antarctic Survey, [5]SUERC

1. Introduction

This study represents the first attempt to constrain the long term evolution of the Antarctic Peninsula Ice Sheet (APIS) in the Larsen Embayment and provides the first terrestrial geological evidence of ice-free areas within the APIS over multiple glacial cycles. The APIS is poorly constrained in terms of its volume and extent at the Last Glacial Maximum (LGM). Current Antarctic Ice Sheet models show complete ice coverage over the Antarctic Peninsula and extensive ice sheet thickening during the Last Glacial Maximum (LGM). However, evidence from biological refugia suggests areas of Antarctica have been ice free for millions of years (Convey *et al.* 1998).

2. Methods

Field investigations were undertaken in the Eternity Range, Northern Palmer Land (Figure 1). A series of glacial erratics and bedrock samples were taken for cosmogenic isotope analysis. Using unstable cosmogenic isotopes ^{10}Be and ^{26}Al and stable cosmogenic isotope ^{21}Ne we reconstructed the deglacial history of this sector of the Antarctic Peninsula.

Figure 1. Location of study highlighted.

By using a unstable multi-isotopic approach we were able to determine:

1) If the area had experienced a simple/ complex deglacial history
2) If the area had been covered in cold ice
3) Erosion rates on the rock surfaces

When low erosion rates were applied to the rock surfaces the oldest samples in the study reached complete isotopic saturation, so cosmogenic ^{21}Ne had to be used to look at the longer-term history of this section of the APIS.

Figure 2. Sampling in the Eternity Range. Geological samples were collected across Mount Faith, Mount Sullivan and Engel Peaks. The "dip-stick" sampling approach was adopted to measure the maximum ice extent and thinning rates of the ice sheet. A total of 39 samples were taken for cosmogenic isotope analysis. This poster shows the results for the 5 highest altitudinal samples only.

3. Results

Geomorphological mapping

Geomorphological mapping in the region identified a Maximum Altitude of Erratics (MAE) in the Eternity Range (Figure 3). Glacial erratics were located towards the summit of Mount Sullivan and on the summits of Engel Peaks (Figure 3). Across the site location deeply weathered and pitted surfaces were identified, which were further exaggerated above the MAE.

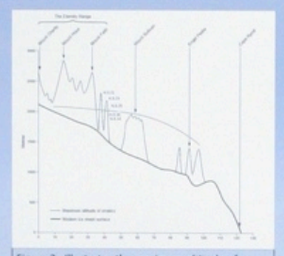

Figure 3. Illustrates the maximum altitude of erratics in the study location. Figure also illustrates the approximate location of samples. For full details of the samples altitude please see Figure 6.

Cosmogenic isotope analysis

^{10}Be and ^{26}Al data suggests a simple record of ice sheet thinning in this region of the Antarctic Peninsula (Figure 4). While ^{21}Ne and ^{10}Be analysis suggests the lower altitudinal samples N.8.18 and N.8.36 have a more complex deglacial history (Figure 5).

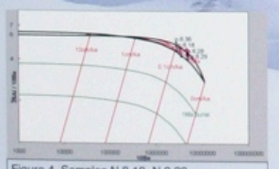

Figure 4. Samples N.8.18, N.8.28, N.8.29, N.8.36 all plot within the "island" suggesting a simple exposure history.

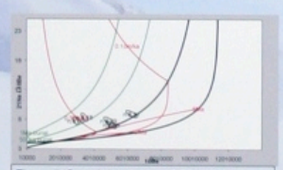

Figure 5. Samples N.8.18, N.8.28, N.8.29, N.8.31, N.8.36. Samples above the MAE (Figures 3 and 6) show simple ice sheet history, while the lower samples show a more complex history.

Sample ID	Altitude (m.a.s.l)	Height above current ice sheet (m)	Exposure age (^{21}Ne results)	Exposure age (^{10}Be, ^{26}Al results)
N.8.31	2229	729	2.8Ma ± 61.3Ka	2.6Ma* ± 467Ka
N.8.29	2142	642	1.9Ma ±57.4Ka	1.3Ma ± 226Ka
N.8.28	2104	504	1.8Ma ± 54.3Ka	1.1Ma ± 171Ka
N.8.36	1969	469	1.1Ma ± 37.1Ka	620Ka ± 86Ka
N.8.18	1952	452	1.4Ma ± 44.4Ka	682Ka ± 77Ka

Figure 6. Exposure ages above and below the Maximum Altitude of Erratics. ^{21}Ne data was calculated in Cosmo-Calc. ^{26}Al and ^{10}Be ages were calculated in Cronus using a time-dependent scaling scheme and Lal and Stone's scaling scheme. Erosion for all samples in Figure 6 are zero. The red line on the table corresponds with the line of maximum erratics shown in Figure 3.
*Sample N.8.31 has not been tested for ^{26}Al, therefore the exposure age shown is calculated using ^{10}Be data only.

Exposure ages obtained from analysis of ^{21}Ne and twinned ^{10}Be, ^{26}Al data above the MAE correspond with each other and suggest areas of the Antarctic Peninsula have remained ice free throughout multiple glacial cycles. ^{21}Ne ages below the MAE are much older than the ^{10}Be, ^{26}Al data suggesting the ^{21}Ne data is picking up an older glacial signal due to ^{21}Ne inheritance in the younger samples.

4. Conclusions

- Summits in the Eternity range have remained ice-free for multiple glacial cycles
- ^{21}Ne data from below the MAE produces older exposure ages compared to ^{10}Be, ^{26}Al exposure ages, suggesting ^{21}Ne inheritance
- This region of the Antarctic Peninsula has experienced much less ice thickening at the LGM than LGM ice extent models suggest

The results from this research suggest that in this sector of the APIS volume changes were far more muted than those recorded on the western fringes. This may reflect precipitation starvation due to the build up of a large independent ice dome over Alexander Island and in the vicinity of George VI Sound. This restricted ice sheet thickening to the east and preserved ice-free areas in this sector of the APIS over multiple glacial cycles.

5. References and acknowledgements

Convey P, Gibson J, Hillenbrand C, Hodgson D, Pugh P, Smellie J, Stevens M (2008). Antarctic Terrestrial life challenging the history of a frozen continent? *Biological Reviews*. **83** 103-117

This work was made possible by the kind generosity and assistance of:
NERC CIAF award 9067,
BAS logistics,
BAS GGS
Antarctic Science Bursary
Dr Anne Le Brocq
Dr Timothy Barrows

For further questions please contact:
Rebecca Rixon
R.N.Rixon@ex.ac.uk
Geography,
University of Exeter,
Amory Building,
Rennes Drive
Exeter
EX4 4RJ
U.K

UNIVERSITY OF EXETER · UNSW · British Antarctic Survey, NATURAL ENVIRONMENT RESEARCH COUNCIL · UNIVERSITY OF CAMBRIDGE · SUERC Scottish Universities Environmental Research Centre

XVIII. INQUA BERN 2011 SWITZERLAND

Poster Award for Monday

Rebecca Rixon

University of Exeter
UK

Sponsor:

Stadt Bern

Exploration and Development of the Climate Archive of the Allan Hills, Antarctica

N.E. SPAULDING[1,2], A.V. Kurbatov[1], P.A. Mayewski[1,2], M.L. Bender[3], J.A. Higgins[3], V.B. Spikes[4], D.A. Introne[1], S.B. Sneed[1]

1. Climate Change Institute, University of Maine, Orono, ME, 04469; 2. Department of Earth Sciences, University of Maine, Orono, ME, 04469;
3. Department of Geosciences, Princeton University, Princeton, NJ 08544; 4. Earth Agency LLC, Stateline, NV 89449

1. Quest for the Oldest Ice

The Allan Hills blue ice area, located on the western flank of the Convoy Range of the Trans-Antarctic Mountains (Figure 1), may be able to provide a high-resolution record of great antiquity suitable for paleoclimate reconstructions. Ages from a micro-meteorite layer embedded in the ice and an individual meteorite indicate that ice as old as 2.5 Ma may be present at the surface. Radiometric terrestrial ages of meteorites and ice flow rates based on strain grids suggest continuous ice ages of 0-1.0 Ma.

Multi-million year records from marine sediments have hinted at possible drivers of climate, but their relatively low resolution and lack of direct proxies for reconstructing atmospheric chemistry make deciphering the interactions between these drivers difficult. Increased resolution and direct atmospheric proxies are available in ice cores; however, the longest existing record (EPICA Dome C (EDC)) only reaches 800 ka. Extending this record will greatly aid efforts to elucidate the factors controlling climate dynamics.

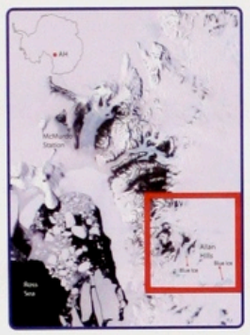

Figure 1: The Allan Hills Blue Ice Area is an anomalous mass-loss region within the accumulation zone of the East Antarctic Ice Sheet. Here sub-surface topography redirects slowly moving deep ice to the surface, where slope and strong katabatic winds combine to expose old ice.

2. Surface Ice Sampling

An estimated ice flow path through the Allan Hills Main Ice Field (MIF) was established in 2004 using topography produced from kinematic GPS surveying. In order to determine if surface ice along that path contained an undisturbed sequential environmental record, chips of ice were collected from 3-4cm depth every 10m along the flowline in the manner shown at right (Figure 2).

Those samples were analyzed for $\delta^{18}O$ and the results of those analyses are shown in Figure 3.

Figure 2: Chips of surface ice are collected in the Allan Hills Blue Ice Area. The ice appears blue because solar radiation is absorbed in the red part of the spectrum and reflected in the blue. The lightness of the color results from uniform scattering of light by enclosed bubbles.

***Note the presence of mountains and nunataks in the photo background. These feautures and their sub-surface counterparts allow old ice to be directed to the surface and sit stagnant for long periods of time.*

3. Oxygen Isotopic Composition and Chemical Analysis

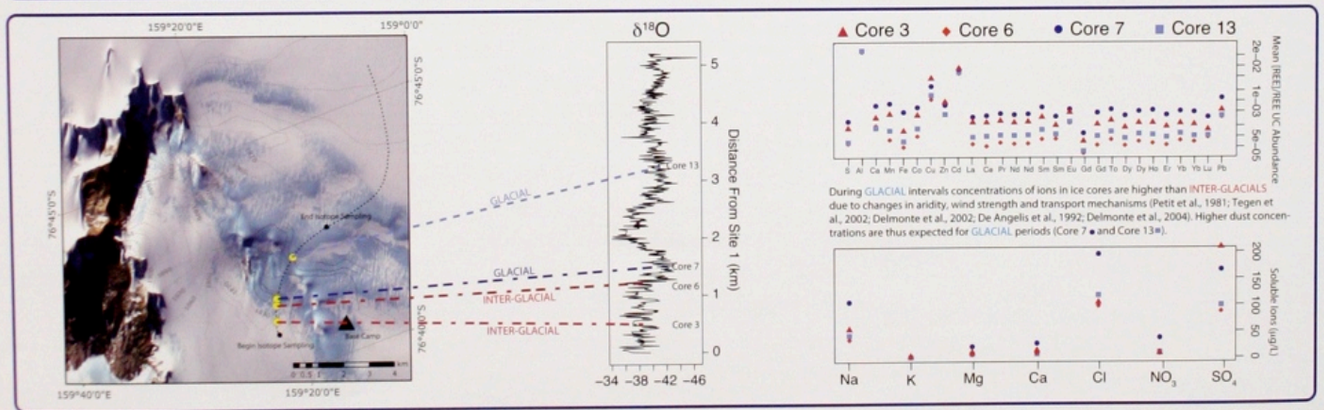

Figure 3: Surface samples were collected every 10m along the the estimated flowline (dotted path) in the Allan Hills MIF. Direction of ice flow is roughly from the upper right to lower left of the image, with ice being near stagnant closest to the nunatak. Yellow dots indicate the location of shallow cores analyzed for soluble ion and trace element chemistry.

During GLACIAL intervals concentrations of ions in ice cores are higher than INTER-GLACIALS due to changes in aridity, wind strength and transport mechanisms (Petit et al., 1981; Tegen et al., 2002; Delmonte et al., 2002; De Angelis et al., 1992; Delmonte et al., 2004). Higher dust concentrations are thus expected for GLACIAL periods (Core 7 ● and Core 13■).

In central East Antarctica, the transition from glacial/inter-glacial conditions is recorded by a 5 ‰ or more increase of the abundance of $\delta^{18}O$ in the ice over a relatively short depth interval. The range of the $\delta^{18}O$ values within the 536 samples analyzed fits this observation and are similar to those found in the glacial/inter-glacial cycles of the Vostok, Taylor Dome, and EDC cores (Figure 4), suggesting that intelligible information about the climate history or structure of the ice sheet is preserved within the surface ice of the Allan Hills MIF. This is partially confirmed by ice core chemistry as those ice cores collected from glacial sections of the path have higher dust concentrations than the inter-glacial sections (with the exception of Core 3). More sections from a second season of collection will be analyzed in coming months.

4. Ice Coring and Future Work

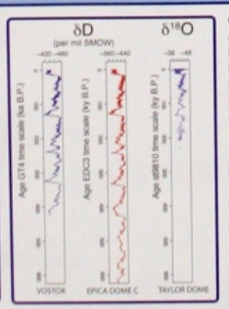

One of the main challenges of the project will be to determine an accurate chronology along the flowline. To accomplish this task a multi-prong approach is being used. $^{40}Ar_{ATM}$ measurements are being carried out at Princeton University, radiometric meteorite ages are being incorporated in a simple ice-flow model, and tephra layers that intersect the flowline are being dated. Additionally, a 225-meter ice core was drilled at a bedrock high along the flowline and a 15 cm resolution $\delta^{18}O$ profile is being created from that core. By matching that profile with the surface profile in Figure 3 and with deep core profiles, such as those at left, a relative time-scale can be determined. Chemical analysis of selected sections of the 225-meter core will also be conducted.

Figure 4 (Far Left): Ice coring in the Allan Hills.

Figure 5 (Left): Down core isotope records from Vostok, Taylor Dome and EDC.

Figure 6 (Right): Cartoon version of how surface isotope record will be matched with forthcoming down-core isotope record.

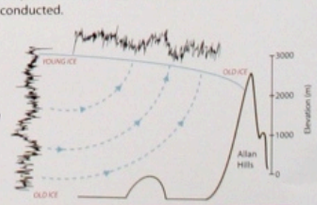

5. References and Acknowledgments

Harvey, R. P., Dunbar, N. W., McIntosh, W. C., Esser, R. P., Nishiizumi, K., Taylor, S., and Caffee, M. W. (1998). Meteoritic event recorded in Antarctic ice. Geology 26, 606-610.

Petit, J.R., J. Jouzel, D. Raynaud, N.I. Barkov, J.M. Barnola, I. Basile, M. Bender, J. Chappellaz, J. Davis, G. Delaygue, M. Delmotte, V.M. Kotlyakov, M. Legrand, V. Lipenkov, C. Lorius, L. Pépin, C. Ritz, E. Saltzman, and M. Stievenard. 1999. Climate and atmospheric history of the past 420,000 years from the Vostok ice Core, Antarctica. Nature 399:429-436.

Jouzel, J., V. Masson-Delmotte, O. Cattani, G. Dreyfus, S. Falourd, G. Hoffmann, B. Minster, J. Nouet, J.M. Barnola, J. Chappellaz, H. Fischer, J.C. Gallet, S. Johnsen, M. Leuenberger, L. Loulergue, D. Luethi, H. Oerter, F. Parrenin, G. Raisbeck, D. Raynaud, A. Schilt, J. Schwander, E. Selmo, R. Souchez, R. Spahni, B. Stauffer, J.P. Steffensen, B. Stenni, T.F. Stocker, J.L. Tison, M. Werner, and E.W. Wolff. 2007. Orbital and Millennial Antarctic Climate Variability over the Past 800,000 Years. Science, Vol. 317, No. 5839, pp.793-797.

Steig E.J. Morse DL, Waddington ED, Stuiver M, Grootes PM. 2000. Wisconsinan and Holocene climate history from an ice core at Taylor Dome, western Ross Embayment, Antarctica. Geografiska Annaler 82A: 213-235.

We thank John Annexstad, Georg Delisle, Ludolf Schultz and John Moore for their previous work in Allan Hills and willingness to share data from those expeditions. We also gratefully acknowledge field assistance from Mike Waszkiewicz, Kristin Schild, Melissa Rohde, Erik Venteris, Leigh Stearns, and the late Ian Whillans. Flights by Kenn Borek Air Ltd. and logistics by Raytheon Polar Services. Funding for this research was provided by the U.S. National Science Foundation Office of Polar Programs through grants 0838843, 0229245, and 9527571.

XVIII. INQUA BERN 2011 SWITZERLAND

Poster Award for Monday

Nicole Spaulding

University of Maine
USA

Sponsor:

Stadt Bern

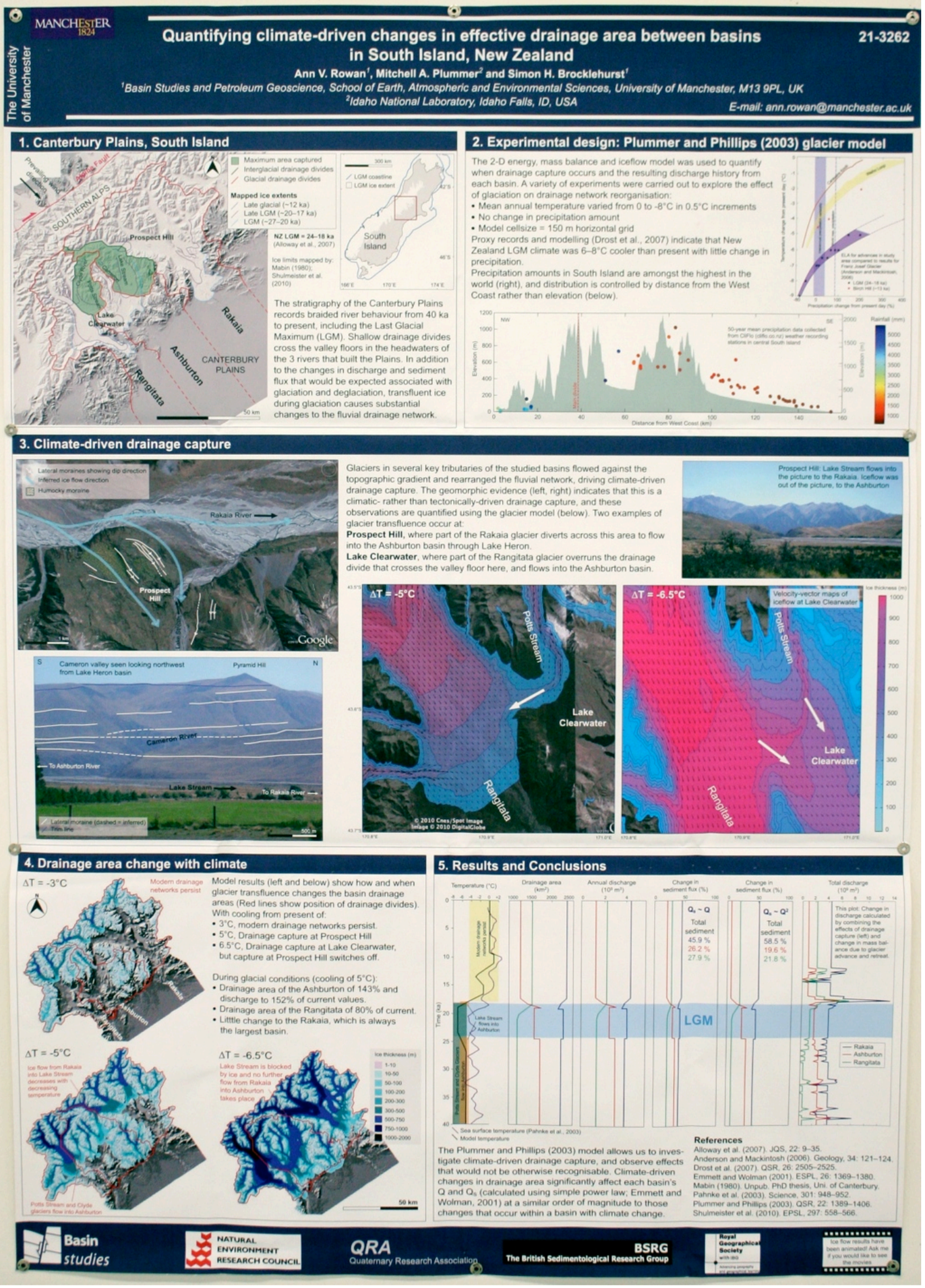

XVIII. INQUA BERN 2011 SWITZERLAND

Poster Award for Monday

Ann Rowan

University of Manchester
UK

Sponsor:

Stadt Bern

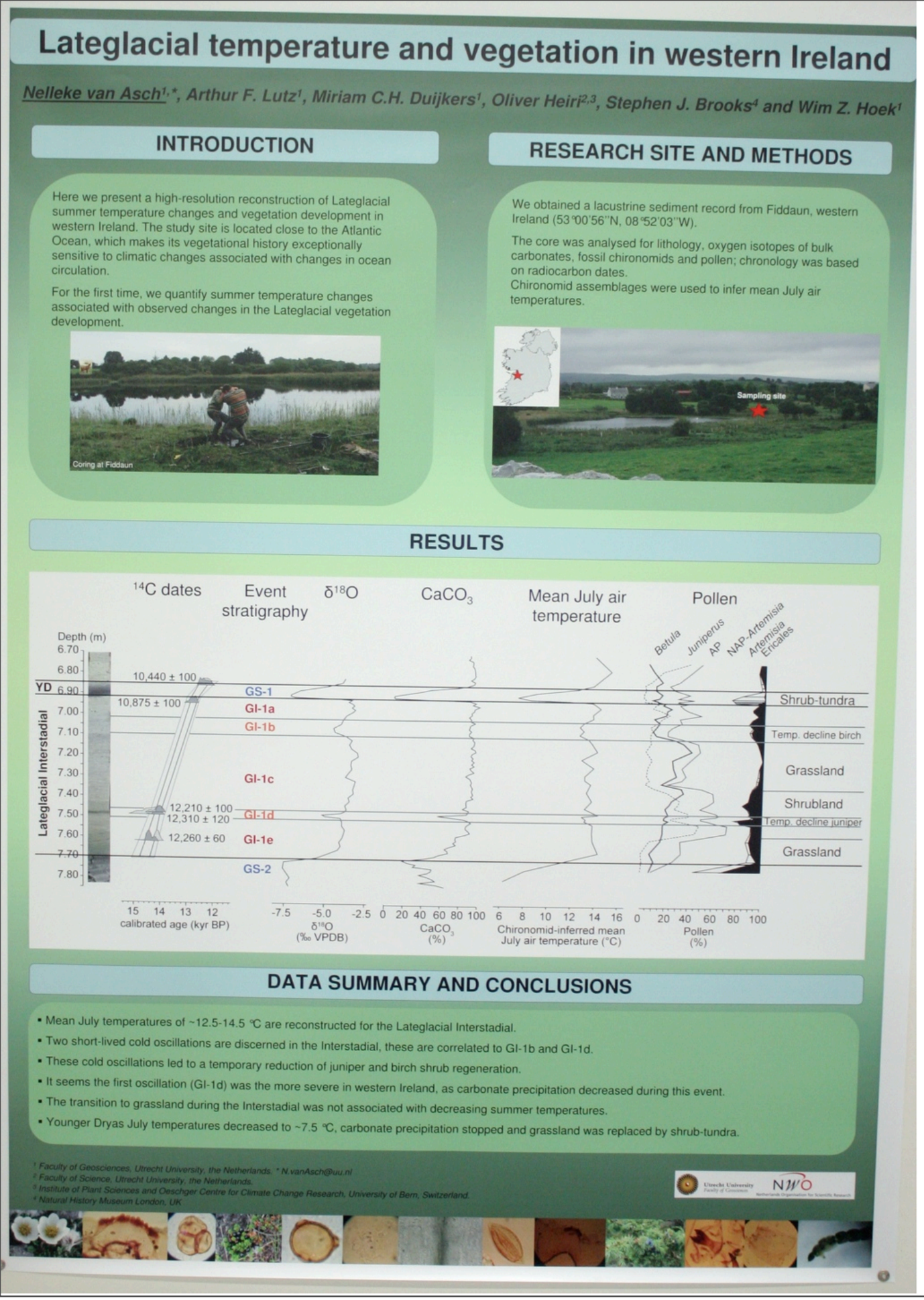

XVIII. INQUA BERN 2011 SWITZERLAND

Poster Award
for
Monday

Nelleke van Asch

Utrecht University
the Netherlands

Sponsor:

Stadt Bern

XVIII. INQUA BERN 2011 SWITZERLAND

Poster Award
for
Tuesday

Presented by Heike Langenberg
Nature Geoscience

The winners are:

Stefanie Wirth
Hongwei Li
Alan Halfen
Achille Mauri

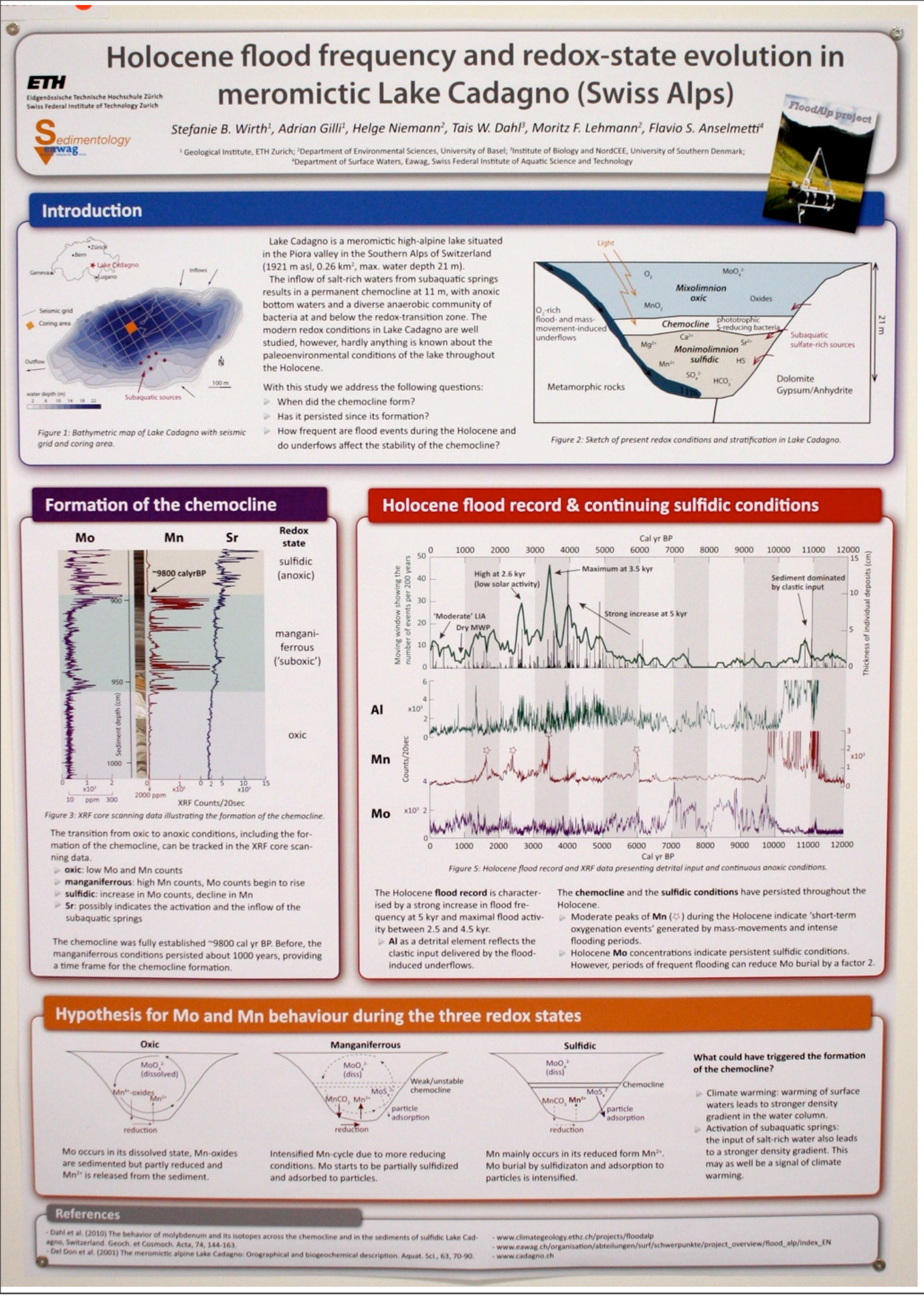

XVIII. INQUA BERN 2011 SWITZERLAND

Poster Award
for
Tuesday

Stefanie Wirth

ETH Zurich
Switzerland

Sponsor:

PAGES
PAST GLOBAL CHANGES

Vegetation Variations in Dryland Systems from 1982 to 2006, with a Special Reference to the District of Xilin Gol, China

Hongwei Li, Xiaoping Yang

Key Laboratory of Cenozoic Geology and Environment, Institute of Geology and Geophysics, Chinese Academy of Sciences, P.O. BOX 9825, Beijing 100029, China

Introduction

Located in the east margin of Gobi Desert, Xilin Gol is a transition region between steppe and desert. Steppe, desert-steppe and sandy land are three main subsystems in this region (Fig. 1). In this study, AVHRR NDVI data, covering from 1982 to 2006 in time, are used to investigate dry land's response of vegetation dynamics to climate change.

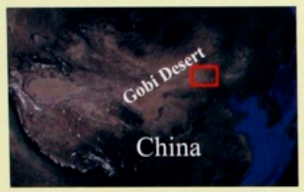

Fig. 1 Location and mean annual growing season (from April to October) NDVI of the study area

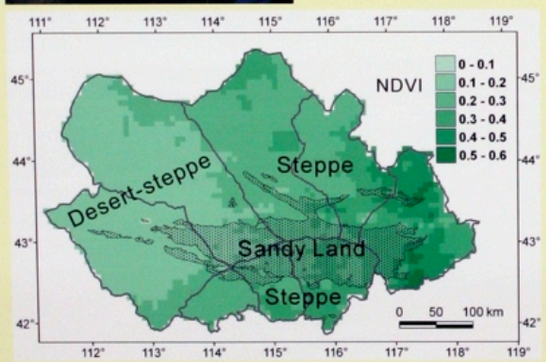

General trend of NDVI

In terms of annual mean growing season NDVI, areas with increasing trend of NDVI are much larger than those with decreasing trend, which are 7% and 0.6%, respectively (Fig. 2).

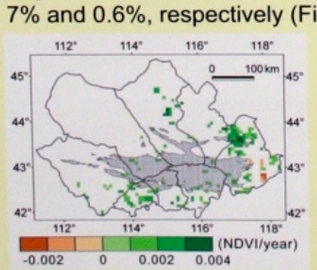

Fig. 2 Significant trend of annual mean growing season NDVI ($p<0.05$)

Factors analysis

Rainfall is the crucial determinant of the NDVI variation, especially to the desert-steppe (Fig 3 A).

In contrast to rainfall, the correlation between NDVI and temperature is negative in the study area (e.g. Fig. 3 C). And the warming trend of the beginning and ending of the growing season would be of benefit to the dryland systems, except for the desert-steppe, (Fig. 3 B and D).

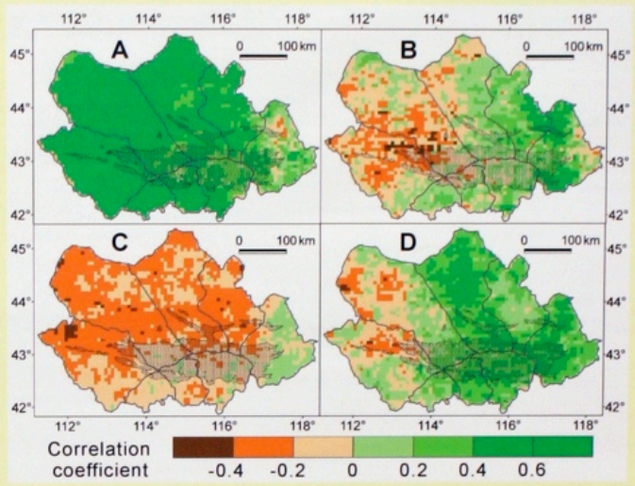

Fig. 3 Correlation between (A) annual rainfall and growing season NDVI, monthly mean temperature and NDVI of (B) April, (C) August, and (D) October.

Stability of the dryland systems

By comparing NDVI dispersion and anomaly degree in response to the fluctuant climate and drought, the stability of the different dryland systems was discussed. It is shown that sandy land is relatively stable in the three subsystems (Fig. 4)

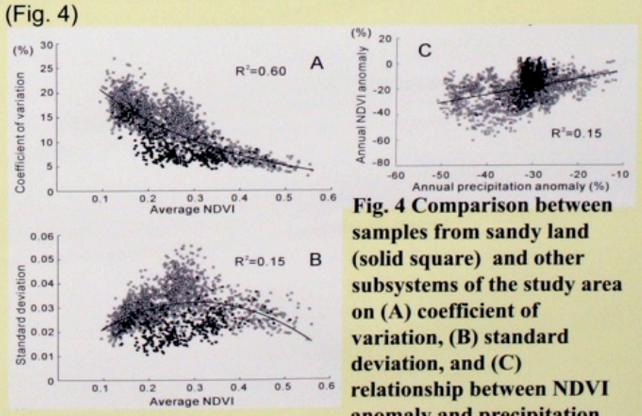

Fig. 4 Comparison between samples from sandy land (solid square) and other subsystems of the study area on (A) coefficient of variation, (B) standard deviation, and (C) relationship between NDVI anomaly and precipitation anomaly in 1989.

Conclusions

Although some area experienced increase of NDVI in the past 30 years, it could not be attributed to the rising temperature occurred in the study area. Generally, the warming trend of the climate would lead to the degradation of vegetation in the dryland systems, and the desert steppe is the most fragile subsystem. Sandy land is the most stable one in the dryland systems. Thus, in the future, much more attention should be paid on the steppe and desert-steppe to control desertification.

XVIII. INQUA BERN 2011 SWITZERLAND

Poster Award for Tuesday

Hongwei Li

Chinese Academz of Sciences
China

Sponsor:

sc | nat

Swiss Academy of Sciences
Akademie der Naturwissenschaften
Accademia di scienze naturali
Académie des sciences naturelles

ProClim

Poster: 61-2833

XVIII INQUA-Congress: Bern, Switzerland

Medieval Climatic Anomaly and Little Ice Age Dune Activity in the Arkansas River Valley, Central Great Plains, USA

Alan F. Halfen (afhalfen@ku.edu) and William C. Johnson (wcj@ku.edu)
University of Kansas, Department of Geography, 1475 Jayhawk Blvd., Lawrence, KS 66045, USA

Introduction

- The Hutchinson, Great Bend Sand Prairie, and Arkansas Valley dunefields are prominent features in the Arkansas River valley.
- Collectively, these features cover more than 1,000,000 ha.
- In addition, these dunefields span a 400-km east-west precipitation gradient with precipitation decreasing by 360 mm to the west.
- The dramatic precipitation gradient, together with the size and location of these dunefields make them crucial to understanding spatial aspects of Great Plains drought.

Methods

- We present a new chronology of dune activation derived from new AMS ^{14}C, 110 new OSL ages, and previously reported ages.

12m section exposing dune and alluvial stratigraphy in the Arkansas Valley Dunefield [left]. Bucket augering for optical dating samples in the Hutchinson Dunefield [right].

Arkansas River Valley

Chronological Results

- Age results indicate that dunefields in the Arkansas River valley were active during the early to middle Holocene.
- The vast majority of dune activation ages from the Arkansas River valley are younger than 2000 cal. yrs B.P.
- Of those ages, most are younger than 500 cal. yrs B.P.
- This pattern suggests that younger episodes of dune activity have overprinted much of the older episodes of activity.

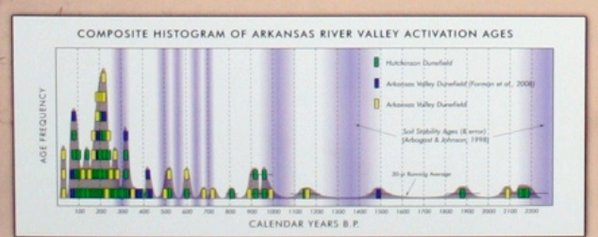

- Further evidence of younger dunes overprinting older dunes can be observed in the individual morphology of many dunes in the Arkansas Valley Dunefield.

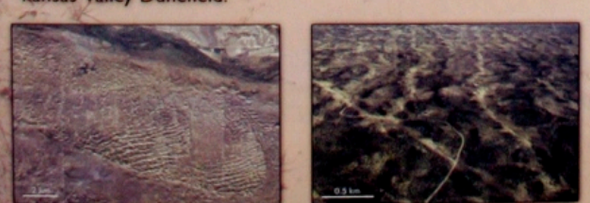

Topdown [left] and oblique [right] views of transverse dunes in the Arkansas Valley Dunefield. Younger, south-trending parabolic dunes are mostly overprinting older, south-trending transverse dunes in both images.

Climatological Implications

- Dune activity in the Arkansas River Valley appears to be coeval with major climatic shifts, most notably, the Medieval Climatic Anomaly and the Little Ice Age.

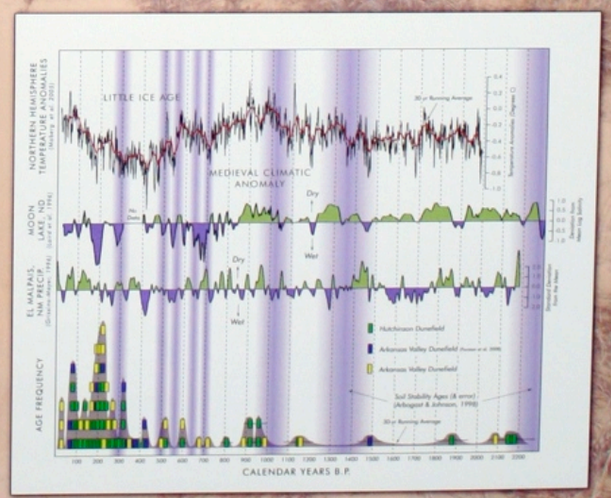

Acknowledgements

We would like to acknowledge Paul Hanson (University of Nebraska-Lincoln) and Joel Spencer (Kansas State University) for assisting in the production of the optical ages used in this presentation. We would also like to thank Terri Woodburn for assistance in the field. Finally, we thank the numerous landowners who provided sampling access. This project was funded by the National Science Foundation (SBE-1030254), the United State Geological Survey EDMAP and STATEMAP Programs, the Geological Society of America, the American Philosophical Society, and the University of Kansas.

XVIII. INQUA BERN 2011 SWITZERLAND

Poster Award for Tuesday

Alan Halfen

University of Kansas
USA

Sponsor:

nature geoscience

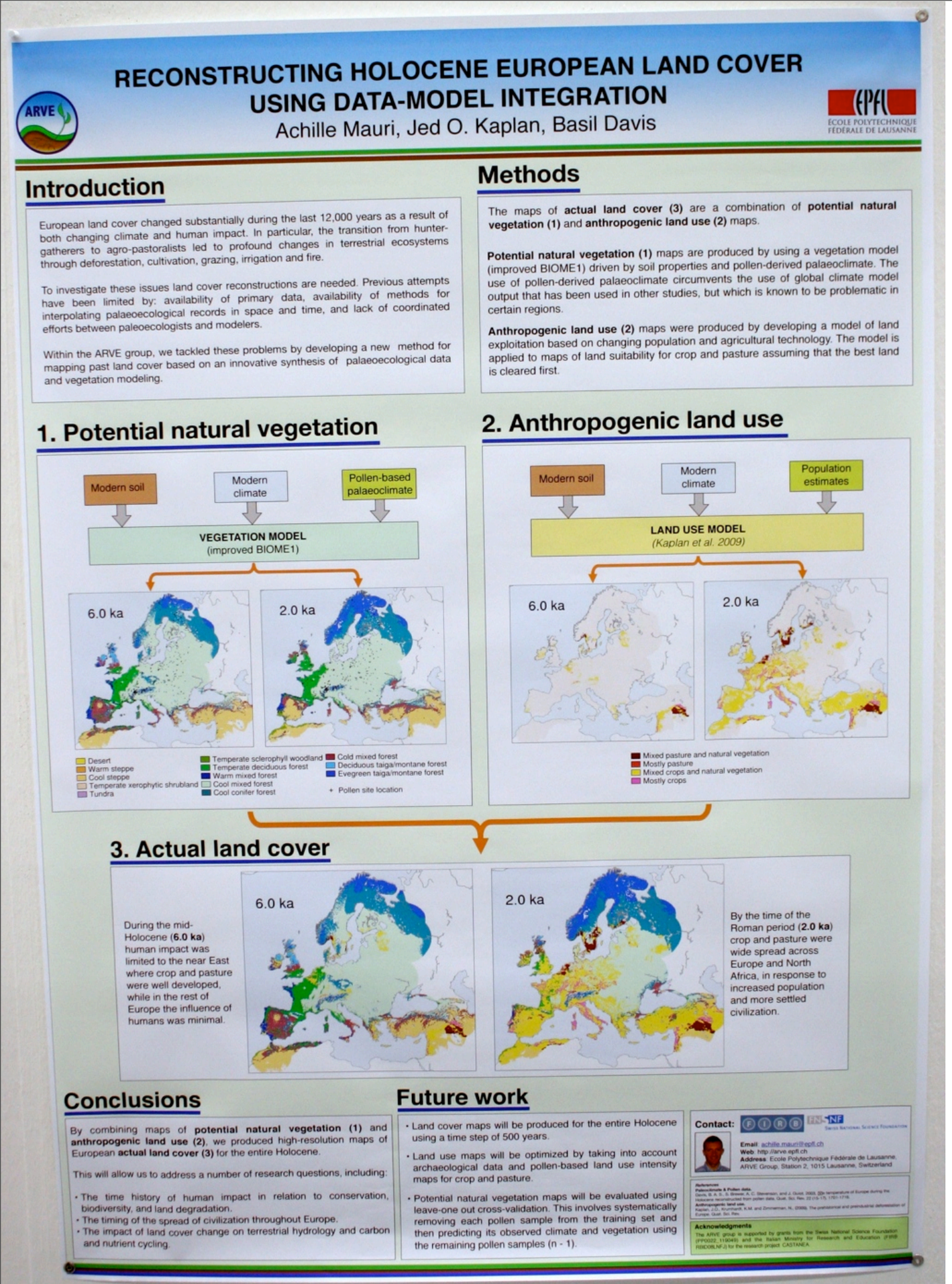

XVIII. INQUA BERN 2011 SWITZERLAND

Poster Award for Tuesday

Achille Mauri
EPF Lausanne
Switzerland

Sponsor:

nature geoscience